Petal–like modes in Porro prism resonators

Igor A. Litvin[1,2], Liesl Burger[1,3] and Andrew Forbes[1,3*]

[1]*CSIR National Laser Centre, PO Box 395, Pretoria 0001, South Africa*
[2]*Laser Research Institute, Physics Department, University of Stellenbosch, Stellenbosch 7602, South Africa*
[3]*School of Physics, University of KwaZulu–Natal, Private Bag X54001, Durban 4000, South Africa*
[*]*Corresponding author: aforbes1@csir.co.za*

Abstract: A new approach to modeling the spatial intensity profile from Porro prism resonators is proposed based on rotating loss screens to mimic the apex losses of the prisms. A numerical model based on this approach is presented which correctly predicts the output transverse field distribution found experimentally from such resonators.

OCIS codes: (140.4780) Optical resonators; (260.0260) Physical optics; (140.3410) Laser resonators; (230.5480) Prisms; (140.0140) Lasers and laser optics

References and links

1. G. Gould, S. Jacobs, P. Rabinowitz and T. Shultz, "Crossed Roof Prism Interferometer," Appl. Opt. **1**, 533–534 (1962).
2. I. Kuo and T. Ko, "Laser resonators of a mirror and corner cube reflector: analysis by the imaging method," Appl. Opt. **23**, 53–56 (1984).
3. G. Zhou and L.W. Casperson, "Modes of a laser resonator with a retroreflecting roof mirror," Appl. Opt. **20**, 3542–3546 (1981).
4. J. Lee and C. Leung, "Beam pointing direction changes in a misaligned Porro prism resonator," Appl. Opt. **27**, 2701–2707 (1988).
5. Y. A. Anan'ev, V. I. Kuprenyuk, V. V. Sergeev and V. E. Sherstobitov, "Investigation of the properties of an unstable resonator using a dihedral corner reflector in a continuous-flow cw CO_2 laser," Sov. J. Quantum Electron. **7**, 822–824 (1977).
6. I. Singh, A. Kumar and O. P. Nijhawan, "Design of a high-power Nd:YAG Q-switched laser cavity," Appl. Opt. **34**, 3349–3351 (1995).
7. N. Hodgson and H. Weber, *Laser Resonators and Beam Propagation* (Springer, 2005), Chap. 17.
8. Y. Z. Virnik, V. B. Gerasimov, A. L. Sivakov and Y. M. Treivish, "Formation of fields in resonators with a composite mirror consisting of inverting elements," Sov. J. Quantum Electron **17**, 1040–1043 (1987).
9. T. A. Anan'ev, "Unstable prism resonators," **3**, 58–59 (1973).
10. A. E. Siegman, H. Y. Miller, "Unstable Optical Resonator Loss Calculations Using Prony Method," Appl. Opt. **9**, 2729–2736 (1970).

1. Introduction

Right angle prisms, often referred to as Porro prisms, have the useful property that all incident rays on the prism are reflected back parallel to the initial propagation direction, independent of the angle of incidence. Thus an initial planar wave front remains planar after reflection. This property was initially exploited in Michelson interferometers to relax the tolerances on misalignment, and then proposed in 1962 by Gould *et al* [1] as a means to overcome misalignment problems in optical resonators employing Fabry–Perot cavities by replacing the end face mirrors with crossed roof prisms. Lasers based on this principle have been developed over the years [2–6] with a review of the basic concepts and literature for Porro prisms specifically found in [7]. Much of the theoretical work to date has focused on geometric methods to model the inverting properties of such resonators [2–4] and polarization considerations to account for internal phase shifts and output polarization states [6,7]. In [2] the prism was modeled as a ray deviator by replacing an imaginary mirror some distance behind the prism. The model correctly accounted for the beam direction, but did not account for the complex field distribution found experimentally from the laser.

#86809 - $15.00 USD Received 23 Aug 2007; revised 5 Oct 2007; accepted 8 Oct 2007; published 11 Oct 2007

Even the physical optics models fail to account for the true field pattern found from such resonators [3,8]. In [3] for example, the kernel of the Fresnel–Kirchoff diffraction integral contains only the optical path length experienced by the beam, thus treating the prism as though it were a perfect mirror, with an identical ABCD matrix representation albeit incorporating the inverting properties of the prisms. This approach appears to be the preferred model for prisms [7], even though it does not explain the complex transverse field patterns found in Porro prism resonators. This is a recurring problem in the literature, with only a hint at a solution offered in [8] and [9], where it was proposed to treat the field patterns as a result of diffractive coupling between a linear combination of sub-resonators. Anan'ev [9], in considering the theoretical properties of resonators with corner cube prisms, specifically mentioned the influence of bevels of finite width at the prism edges as a possible explanation for a tendency for distinct longitudinal sectors to oscillate independently, but did not go on to develop this idea into a model which could be used to explain experimental results.

In this paper we propose a new method for modeling the transverse field patterns observed from crossed Porro prism resonators. The model departs from earlier attempts in that the prisms are modeled as rotating elements with amplitude and phase distortions, and incorporates both physical optics and geometrical optics concepts. The model is developed in section (2) and its properties discussed, and then applied in section (3) to the case of a marginally stable crossed Porro prism resonator with a polarizer as an output coupler.

2. Porro resonator concept

A typical Porro prism resonator is shown in Fig. 1. Consider for the moment only the two Porro prisms and how they impact on the propagating field. Imagine viewing the resonator along its length from one prism (element ***h***) looking towards the other (element ***a***). On encountering a prism, the field inverts around the prism apex, and reverses its propagation direction, traveling back towards the opposite prism. The same inversion and reversal of propagation direction takes place again, and this sequence repeats on each pass. The prisms would essentially be treated as perfect mirrors but with a field inverting property.

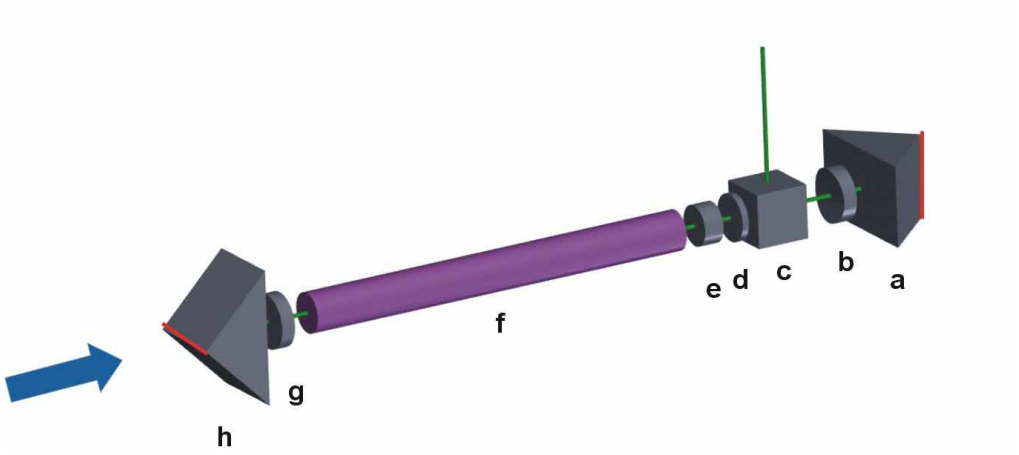

Fig. 1. A typical Porro prism based Nd:YAG laser with passive Q–switch, showing the following optical elements: Porro prisms (elements a and h); intra–cavity lenses (elements b and g); a beamsplitter cube (element c); a quarter wave plate (element d), and a passive Q–switch (element e).(interactive pdf 117 KB)

Our approach to modeling a resonator containing Porro prisms is to describe the prisms as standard mirror elements, but with associated amplitude and phase screens, as illustrated in Fig. 2. These screens act on the incoming field by modifying both its amplitude and phase by means of a suitable optical transfer function $t(x,y)$:

#86809 - $15.00 USD Received 23 Aug 2007; revised 5 Oct 2007; accepted 8 Oct 2007; published 11 Oct 2007

$$U_{out}(x,y) = U_{in}(x,y)t(x,y) = U_{in}(x,y)A(x,y)\exp(i\varphi(x,y)), \quad (1)$$

where $A(x,y)$ describes the amplitude effects and $\varphi(x,y)$ describes the phase effects of the prism. In the case of a Porro prism, the amplitude screen introduces losses not only at the edges of the element (transverse confinement), but also at the small but significant bevel along the apex where the prism surfaces meet. The phase screen allows the optical path length to vary as a function of the input position on the prism face, for example, to model errors in the prism angle or fabrication errors on the prism surfaces. With this approach, the diffractive effects of the prisms are taken into account, and the screens can be treated as intra–cavity elements that change the eigenmodes of a standard mirror–mirror resonator. In this paper we employ only the amplitude screen approach to model perfect prisms with high losses where the prism edges meet. The transfer function for the new prism model then includes only the amplitude effects, $t(x,y) = A(x,y)$, and describes a high loss region along the apex of the prism, with 100% losses, and no losses elsewhere within the clear aperture of the element.

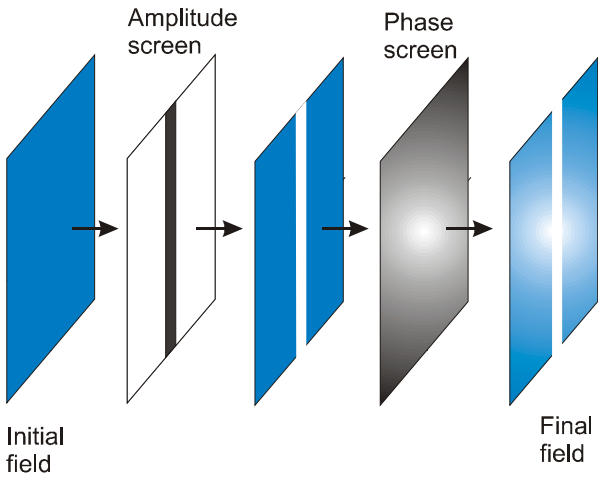

Fig. 2. Illustration of the effect of phase and intensity screens on an incident field.

A geometric approach is useful in understanding the symmetry and repeatability of the resonator modes: consider a propagating ray viewed along the optical axis and assume, without any loss of generality, that the Porro prism (PP) closest to the observer has its apex in the horizontal plane, while the opposite PP has its apex rotated at some angle α from the horizontal, which we will refer to henceforth as the *Porro angle*. By way of example, we consider the case of $\alpha = 60°$, as illustrated in Figs. 3(a)–3(e). In the analysis to follow the pertinent information is the location of the prism apexes, which we illustrate as solid lines 1 and 2 in Fig. 3(a), corresponding to elements ***h*** and ***a*** in Fig. 1 respectively.

#86809 - $15.00 USD Received 23 Aug 2007; revised 5 Oct 2007; accepted 8 Oct 2007; published 11 Oct 2007

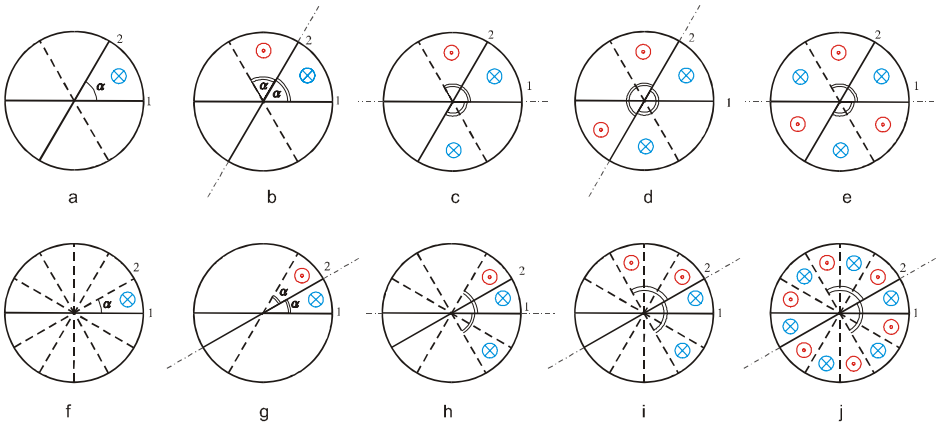

Fig. 3. (a) – (e): Evolution of a ray as it is reflected back and forth in the resonator, for starting Porro angle $\alpha = 60°$. After 3 round trips the pattern is complete (e) and starts to repeat. (f) – (j): Equivalent case but with $\alpha = 30°$, and now taking 6 round trips for completion.

We have *a priori* knowledge of how the mode will develop, and hence start with a ray located as shown in Fig. 3(a), traveling away from the viewer towards PP 2. We have chosen this location based on the assumption of high loss along the apexes, thus avoiding the apex zones. At PP 2 the ray is inverted about the prism apex, and travels back towards the viewer parallel to the optical axis as indicated in Fig. 3(b). At PP 1, the ray is inverted about the prism axis, and travels back towards PP 2 [Fig. 3(c)]. This process continues until the complete pattern is created [Fig. 3(e)], and the ray has returned to its starting position. This happens after three round trips. Clearly subsequent reflections simply duplicate the pattern. A second example is shown in Figs. 3(f)–3(j), where we illustrate the case of $\alpha = 30°$. The same propagation rules apply so that eventually, after six complete round trips the pattern starts repeating itself. Clearly this approach correctly predicts the observed petal pattern formation often observed from such lasers, but this is based on *a priori* knowledge and not physical reasoning. Also, this approach is only useful for limited Porro angles.

An alternative approach, which is more useful in modeling such a resonator, is to consider that since losses are introduced onto the field from each prism apex, and the field is then inverted, one can view the situation as the amplitude screen being inverted after each prism reflection. From the viewpoint of the field traveling inside the resonator, the equivalent picture is that of the field remaining inversion free, while the prisms themselves invert after each pass, essentially appearing to rotate by an amount dependent on the Porro angle, and hence the main area of losses (the apex edges) also appear to rotate. An example of this rotation is shown in Fig. 4.

#86809 - $15.00 USD Received 23 Aug 2007; revised 5 Oct 2007; accepted 8 Oct 2007; published 11 Oct 2007

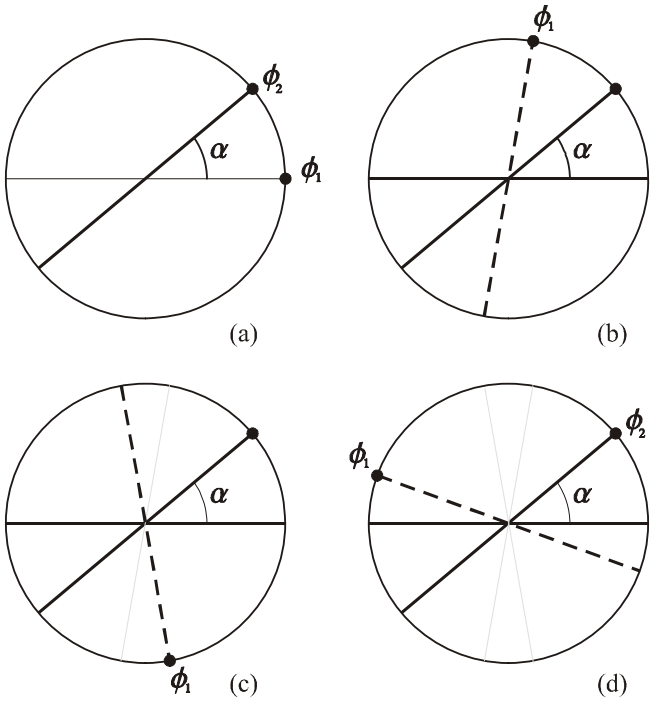

Fig. 4. The apexes of two Porro prisms at angles ϕ_1 and ϕ_2. Initially the apex of PP 1 is in the horizontal plane (a), but after successive reflections about the inverting edges of the two prisms the apex will appear to be rotating about the circle: (b) 1 pass, (c) 2 passes and (d) 3 passes.

In order to develop a physical optics model based on this approach, we need to have expressions for the equivalent picture of the rotating prism apexes (high loss areas). Consider the rotation of the first PP apex, which we shall denote with the subscript 1, whose position on the circle in Fig. 4 we describe by the vector $v_1 = (x_1,y_1)$ with angular displacement given by ϕ_1. The region of high loss is then simply a line passing through the origin with slope y_1/x_1. Without any loss of generality we will assume the resonator is viewed such that the first PP has an edge parallel to the horizontal axis, with the second PP rotated at the Porro angle, as illustrated in Fig. 1. It is easy to show that after n reflections this vector has rotated through an angle $\theta_1(n)$ given by:

$$\theta_1(n) = (-1)^{n+1} 2n\alpha\,, \tag{2}$$

where α is the Porro angle. The angular position of this vector after n reflections can be found from:

$$\phi_1(n) = \sum_{i=0}^{n} \theta_1(i) = \frac{\alpha}{2}\left[1-(-1)^n(1+2n)\right]. \tag{3}$$

Prior to any reflections the apex of the first prism is at $\phi_1(0) = 0$, so that if we imagine the apexes rotating about the unit circle, then the vector $v_1(n)$ may be expressed as:

$$v_1(n) = \begin{pmatrix} \cos\phi_1(n) & -\sin\phi_1(n) \\ \sin\phi_1(n) & \cos\phi_1(n) \end{pmatrix} \begin{pmatrix} 1 \\ 0 \end{pmatrix}. \tag{4}$$

#86809 - $15.00 USD Received 23 Aug 2007; revised 5 Oct 2007; accepted 8 Oct 2007; published 11 Oct 2007

Similar expressions can be derived for the second PP apex, which we state here for the convenience of the reader:

$$\theta_2(n) = (-1)^n 2n\alpha\,; \tag{5}$$

$$\phi_2(n) = \alpha - \frac{\alpha}{2}\left[1-(-1)^n(1+2n)\right]; \tag{6}$$

$$v_2(n) = \begin{pmatrix} \cos\phi_2(n) & -\sin\phi_2(n) \\ \sin\phi_2(n) & \cos\phi_2(n) \end{pmatrix}\begin{pmatrix} 1 \\ 0 \end{pmatrix}. \tag{7}$$

Note that the notation has been selected so that the initial positions of the two apexes are given by:

$$v_1(0) = \begin{pmatrix} 1 \\ 0 \end{pmatrix}, \tag{8a}$$

$$v_2(0) = \begin{pmatrix} \cos\alpha \\ \sin\alpha \end{pmatrix}, \tag{8b}$$

with corresponding initial apex loss regions along $y_1 = 0$ and $y_2 = (\tan\alpha)\, x_2$ respectively.

A consequence of this model is that only at some discrete starting angles α will the rotating edges repeat on themselves, a necessary condition for a mode to be resonant inside the cavity. At these angles the field is finitely sub–divided by the prisms losses, and it takes a certain number of passes for the sub–division of the field to be complete. The resulting field is then made up of a circular pattern of spots which we refer to as petals or as a petal pattern. At other angles, the edges never repeat on themselves, thus infinitely sub–dividing the field. With this formalism we are able to find the angles α at which these repeating patterns manifest themselves, as well as the number of sub–divisions (or equivalently, number of petals) that will be observed. Consider for example the first Porro prism apex. It will return onto itself when $v_1(n) = v_1(0)$, which leads from Eq. (4) to the relation:

$$\begin{pmatrix} \cos\phi_1(n) & -\sin\phi_1(n) \\ \sin\phi_1(n) & \cos\phi_1(n) \end{pmatrix} = \begin{pmatrix} 1 & 0 \\ 0 & 1 \end{pmatrix}. \tag{9}$$

This will be true when

$$\phi_1(n) = \frac{\alpha}{2}\left[1-(-1)^n(1+2n)\right] = i2\pi\,, \tag{10}$$

for any integer i. By selecting only the positive solutions for α one can derive a simple expression for the initial angles α that will lead to a finitely sub–divided field (or repeating pattern from the geometric viewpoint):

$$\alpha = \frac{i\pi}{m}, \tag{11}$$

for any positive integers i and m. The same result can be derived by starting from vector v_2. The implication is that only at these specific angles α will the field be finitely sub–divided, thus leading to some regions with low loss for lasing. In addition, since the position of these sub–divisions remains stable (i.e., they repeat on themselves) after a certain number of round trips, the modal pattern that oscillates inside such a resonator will give rise to a petal pattern *only* at those angles given by Eq. (11). At other Porro angles the high loss apexes will continuously rotate to new positions, thus resulting in high losses across the entire field. We

#86809 - $15.00 USD Received 23 Aug 2007; revised 5 Oct 2007; accepted 8 Oct 2007; published 11 Oct 2007

can now go on to calculate how many petals will be observed for a given Porro angle α. The number of petals will be equal to the number of sub–divisions of the field, but the field may not be completely sub–divided in one complete rotation of the vector; it may take several complete rotations for this to happen. We note that the sub–divisions will not necessarily be equal to the Porro angle; when several rotations of around the circle are needed to complete the sub–divisions, then the area between the initial apexes will be sub–divided further. In general we can write the following expression relating the Porro angle to the total number of sub–divisions (petals) of the field:

$$\frac{\alpha}{j} = \frac{2\pi}{N}. \tag{12}$$

The validity of this is evident from the following heuristic argument: The complete circle (2π) divided by the total number of sub–divisions N must return the angle of each sub–division. If the sub–division is completed in one rotation, then the sub–division angle will equal α, but if more complete rotations are needed, then this will result in α itself being sub–divided by integer amount, j. Thus both the left and right hand sides of Eq. (12) represent the same quantity – the final angle of each sub–division. A simple rearrangement of this equation then yields:

$$N = \frac{j2\pi}{\alpha}. \tag{13}$$

Since each reflection may only increase the number of sub–divisions in multiples of two, we deduce that N must be an even number. The positive integer j now appears to take on the meaning of the number of complete cycles required to return the apexes back onto one another. At present we cannot offer a simple analytical method of determining j, but can offer the following conditions: (i) j is the lowest positive integer such that N is even, and (ii) $j \leq i$.

Equations (11) and (13) are predictions as to which initial angles α will result in stable petal pattern output, and how many petals will be observed in the pattern respectively. A plot of the allowed angles for petal pattern formation together with the number of petals that will be observed is shown in Fig. 5.

Since the sub–divisions divide the circle finitely, the angle subtended by each sub–division is given by:

$$\psi = \frac{2\pi}{N} = \frac{\alpha}{j}. \tag{14}$$

Thus the more complete rotations needed to complete the pattern, the smaller the angle of each sub–division. The simplest case is when $i = 1$; then $j = 1$ and the circle is divided into divisions of α. For higher j values the lossless regions between the high loss sub–division lines become small. Thus although there is an infinite number of solutions for α that lead to finite sub–divisions of the field, if the number of divisions is too large, diffraction will blur the spot structure and no petal pattern will be observed.

#86809 - $15.00 USD Received 23 Aug 2007; revised 5 Oct 2007; accepted 8 Oct 2007; published 11 Oct 2007

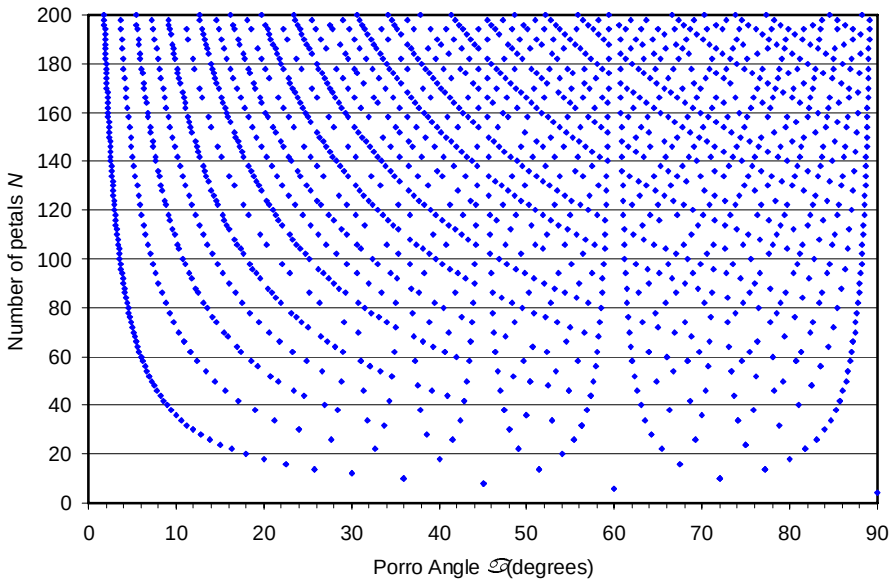

Fig. 5. Plot of the discrete set of angles α that give rise to a petal pattern, with the corresponding number of petals to be observed. Data calculated for $m \in [1,100]$ and $i \in [1,50]$.

Taking this into account, and considering the diffraction of a field propagating between areas of high losses, it is reasonable to suppose that the approach and theory presented here is the explanation for the observed (and sometimes not observed) petal patterns from Porro prism resonators. The governing equations for the onset of petal patterns and the number of petals observed are given by Eqs. (11) and (13) respectively.

3. Test resonator

The Porro prism resonator investigated in this study is shown schematically in Fig. 1, and was based on a flash lamp pumped Nd:YAG laser with passive Q–switching. The active medium was a 50 mm long Nd:YAG rod of radius 3 mm. Two Porro prisms at either end of the laser formed the resonator, replacing traditional mirrors. The stability of the resonators was determined by the two intra–cavity lenses near the prisms, but in our experiment as well as in the numerical model no intracavity lenses were used, yielding a marginally stable resonator. The resonator was confined in the transverse direction by the clear aperture of the optical elements, such as lenses, prisms and gain rod, but also by inserted apertures not shown in the figure. The laser was pulsed using a Cr^{4+}:YAG passive Q–switch. A quarter wave plate together with a polarizing beamsplitter cube ensured variable output coupling from the laser by polarization control (by rotation of the waveplate or by rotation of the prisms).

3.1 Experimental set-up

The assembled laser used in our experiments is shown in Fig. 6. The spatial intensity profile of the laser output was measured using a CCD camera (model COHU 4812). The temporal characteristics were detected with a silicon detector coupled to a 50 Ω impedance, and displayed on a two channel oscilloscope (Tektronic TDS 360).

#86809 - $15.00 USD Received 23 Aug 2007; revised 5 Oct 2007; accepted 8 Oct 2007; published 11 Oct 2007

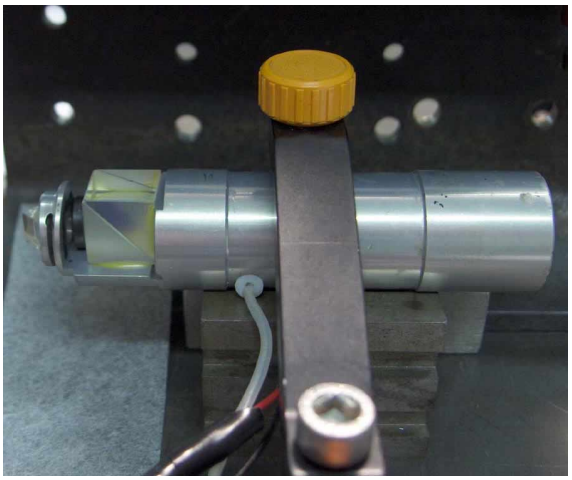

Fig. 6. Photograph of assembled laser. The beamsplitter cube and one of the Porro prisms can be made out on the left of the assembly.

3.2 Numerical modeling

The laser was modeled as the complete resonator *sans* any gain using the Prony method [10]. A beam array size of 1024×1024 was used, and the modal build–up modeled until the losses per round trip stabilized to within 0.5%. The Porro prism resonator was modeled by successive passes through a folded–out resonator using the approach described in section (2). Each prism was assumed to be equivalent to a perfect mirror superimposed on a rotating loss line (see Fig. 2), with the rotation of the loss region for prism 1 given by Eq. (3) and that for prism 2 by Eq. (6).

4. Results and discussion

Using Eqs. (11) and (13), the finite sub–division of the field is predicted at angles $\alpha = 67.5°$ and $\alpha = 77.14°$, with associated petal numbers of 10 and 14 respectively. No finite sub–division is expected at $\alpha = 79.0°$. These cases are shown in Figs. 7(a)–7(c) respectively, where the locations of the prism apexes are shown around the unit circle after several hundred rotations. In insets (a) and (b) the apexes are clearly repeating on themselves, resulting in a stable pattern, whereas in (c) the field does not result in any lossless regions because of the non–repeating apex positions. This latter situation prohibits the formation of a stable mode since all regions have high loss, while the former scenarios could potentially support lasing in the lower loss regions of the field.

The numerical model of the resonator confirms this [see Figs. 7(d)–7(f)], showing a stable mode pattern for $\alpha = 67.5°$ and $\alpha = 77.14°$, with the correct number of petals (10 and 14 respectively) as predicted by the theory. At $\alpha = 79.0°$ the output mode never stabilizes and results in a random field with high losses. Experimental results verify these findings, with petal patterns occurring when they should ($\alpha = 67.5°$ and $\alpha = 77.14°$), and with the correct number of petals: 10 and 14 respectively [see Fig. 7(g) and (h)]. At $\alpha = 79.0°$ no petal pattern was observed experimentally, in agreement with the theory and numerical model, with the camera image showing the time averaged intensity from the laser. Thus the theoretical, numerical and experimental results are all in very good agreement.

#86809 - $15.00 USD Received 23 Aug 2007; revised 5 Oct 2007; accepted 8 Oct 2007; published 11 Oct 2007

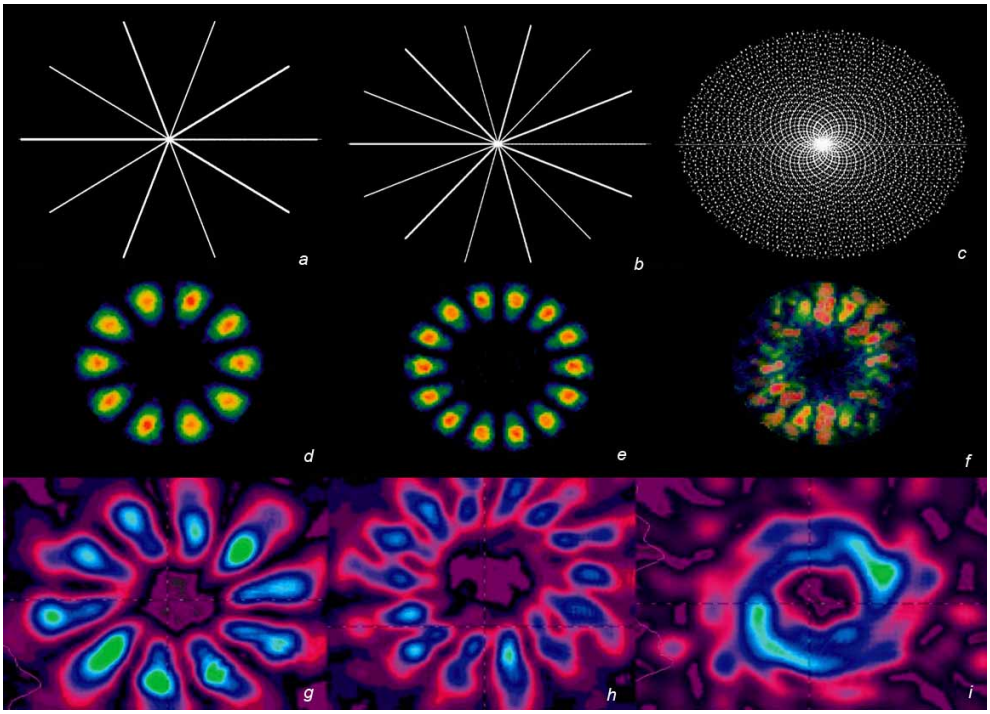

Fig. 7. The analytical model depiction of finitely sub–divided fields in (a) and (b), and an infinitely sub–divided field in (c). Numerically this results in a pattern with (d) 10 petals (movie 3.3 MB), (e) 14 petals (movie 3.5 MB) and (f) no petals (movie 3.4 MB). The corresponding experimentally observed output is shown in (g) – (i).

The angles α for which an output beam existed for the test laser were limited to between 63° and 87°. The absence of output below 63° was due to increased misalignment between the Porro prisms with decreasing angle away from 90° degrees (the crossed case). It should be noted that this was a particular artifact of the resonator under study, and is not a general property of Porro resonators. The absence of output above 87° degrees was due to two effects: (i) the output coupling method of the given cavity: at 90° (crossed Porro prisms) no output existed because cavity losses were 100% due to the polarization based output coupling method; and (ii) near 90° the number of predicted petals increases very rapidly with Porro angle. Since this reduces the available low loss area for the each petal, either no petals are observed due to the inherently high losses, or the close proximity of the petals leads to blurring due to diffraction.

The available experimental data at selected angles α is shown in Table 1, and is in excellent agreement with the theoretical and numerical predictions.

#86809 - $15.00 USD Received 23 Aug 2007; revised 5 Oct 2007; accepted 8 Oct 2007; published 11 Oct 2007

Table 1. Petal pattern observations: theory and experiment

Experiment		Theory	
α	N	α	N
68° ± 0.5°	16	67.5000°	16
72° ± 0.5°	10	72.0000°	10
77° ± 0.5°	14	77.1429°	14
80° ± 0.5°	18	80.0000°	18

In addition to the experimentally verified petals, the numerical model was used for extensive tests on the analytical predictions of section (2). Figure 8 shows examples of some results, with the analytical prediction of the stabilized sub–division of the field shown in the top row, with corresponding petal patterns calculated numerically shown below. The top row of Fig. 8 shows the calculated apex positions after rotation by Eqs. (4) and (7), after a stable pattern has emerged. The model correctly predicts all the salient features of the petal pattern.

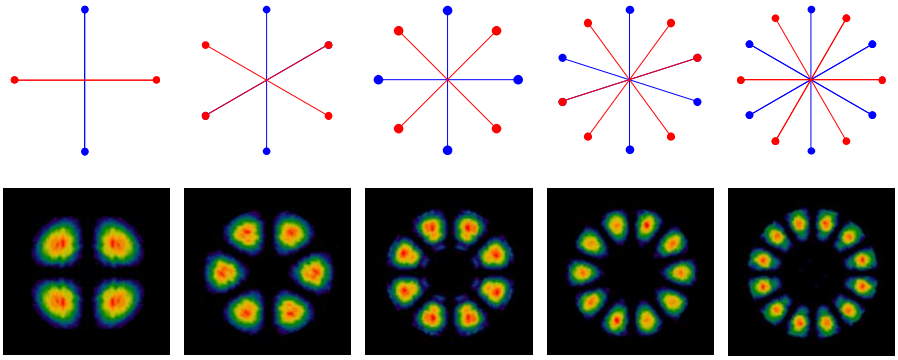

Fig. 8. Analytically calculated sub–division of the field using Eqs. (4) and (7) (top row), with corresponding petal patterns calculated numerically using this model (bottom row).

Associated with an increase in the sub–division of the field is an increase in the loss per round trip inside the laser cavity.

#86809 - $15.00 USD Received 23 Aug 2007; revised 5 Oct 2007; accepted 8 Oct 2007; published 11 Oct 2007

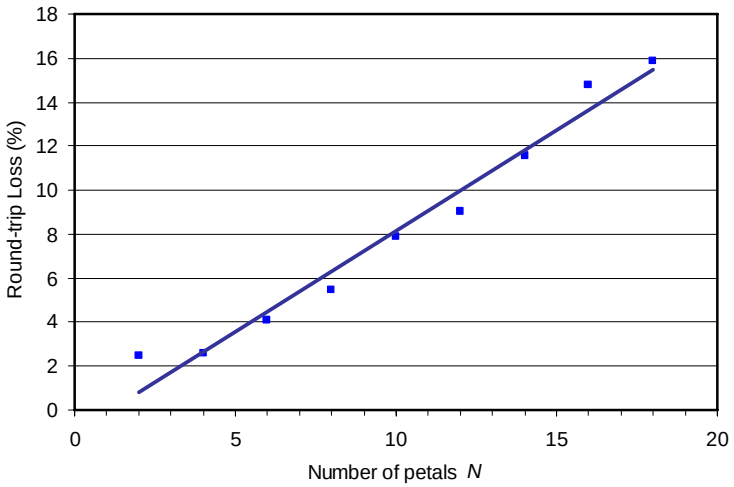

Fig. 9. Plot of the round–trip loss as a function of the number of petals as predicted by the numerical model.

Figure 9 shows that the stabilized round–trip losses increase nearly linearly with the number of petals in the petal pattern over the region that one might reasonably expect to observe petals. This is due to the ever decreasing low loss area as the sub–divisions become closer together. This places restrictions on the allowed Porro angles that can actually be observed experimentally from such lasers.

5. Conclusion

We have presented a new approach to modeling Porro prism resonators that combines geometrical and physical optical aspects. We have shown why such resonators must sometimes generate petal–like patterns, and given the generating equation for the prism angles at which this will happen. The results are confirmed experimentally on a test resonator. The basic premise, that a finite bevel at the apex of the prisms results in losses is true for all such prisms, and thus is a fundamental property of Porro prism resonators.

This work has implications on how such resonators are used in the field. Porro prism resonators are used extensively as range finders, particularly in the military, where their tolerance to misalignment is exploited. In such resonators variable output coupling based on rotating the prisms is often employed, but as has been shown here, this will have a significant impact on the output transverse mode from the laser. Since the transverse mode impacts on beam quality factor and divergence, the choice of operating Porro angle will affect the resulting laser beam propagation to the target as well as far field laser intensity and laser brightness.

Acknowledgments

We would like to thank Denel Optronics for the use of their laser, as well as Mr Johan Steyl, Mr Dieter Preussler and Mr Daniel Esser for useful discussions and advice.

Appendix

By serendipity we noticed that in some experiments a second pulse of energy delayed in time was observed, occurring roughly 25 μs after the first pulse. Further investigation revealed that the occurrence of the second pulse was always associated with a change in the spatial intensity pattern from the resonator. It was found that the observation of the second pulse was a function of the gain of the laser: below a threshold pump level no double pulse was observed,

#86809 - $15.00 USD Received 23 Aug 2007; revised 5 Oct 2007; accepted 8 Oct 2007; published 11 Oct 2007

while above the threshold two pulses were consistently evident. The single pulse intensity profile fits well with the petal model previously described, while the two–pulse time averaged intensity profile is similar to that predicted, but with an additional ring–like structure in the centre of the pattern (see Fig. 10).

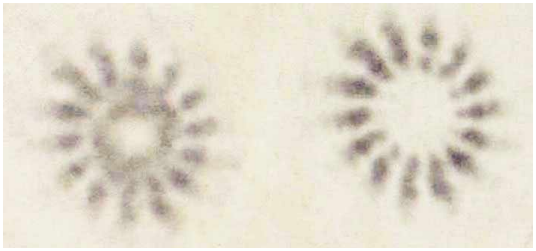

Fig. 10. The transverse field distribution, with (a) two and (b) one pulse. The angle between the Porro prisms is 13° (giving 14 spots).

We suggest that this additional feature in the double–pulse intensity profile can be explained by the fact that the first petal–like pulse leaves a region of excess gain in the centre of the Nd:YAG rod, allowing lasing to continue for modes with much higher losses, hence the delay in output. The continuous band may be due to diffractive smearing of the very close petals. It also hints at the possibility of perhaps more complex modes that can oscillate inside such resonators.

#86809 - $15.00 USD Received 23 Aug 2007; revised 5 Oct 2007; accepted 8 Oct 2007; published 11 Oct 2007